applied sciences

MDPI

Article

Control of Corner Separation with Plasma Actuation in a High-Speed Compressor Cascade

Haideng Zhang [1,2], Xianjun Yu [2,3,4,*], Baojie Liu [2,3,4], Yun Wu [1] and Yinghong Li [1]

1 College of Aeronautical and Aerospace Engineering, Science and Technology on Plasma Dynamics Laboratory, Airforce Engineering University, Xi'an 710038, China; zhanghaideng@126.com (H.Z.); wuyun1223@126.com (Y.W.); liyinghong@163.com (Y.L.)
2 School of Energy and Power Engineering, National Key Laboratory of Science and Technology on Aero-Engine Aero-Thermodynamics, Beihang University, Beijing 100191, China; liubj@buaa.edu.cn
3 National Key Laboratory of Science & Technology on Aero-Engine Aero-Thermodynamics, Beihang University, Beijing 100191, China
4 Collaborative Innovation Center of Advanced Aero-Engine, Beihang University, Beijing 100191, China
* Correspondence: yuxj@buaa.edu.cn; Tel.: +86-10-8231-6455

Academic Editors: Antonio Ficarella and Maria Grazia De Giorgi
Received: 31 March 2017; Accepted: 25 April 2017; Published: 29 April 2017

Abstract: The performances of modern highly loaded compressors are limited by the corner separations. Plasma actuation is a typical active flow control methodology, which has been proven to be capable of controlling the corner separations in low-speed compressor cascades. The main purpose of this paper is to uncover the flow control law and the mechanism of high-speed compressor cascade corner separation control with plasma actuations. The control effects of the suction surface as well as the endwall plasma actuations in suppressing the high-speed compressor cascade flow separations are investigated with numerical methods. The main flow structures within the high-speed compressor cascade corner separation and the development of the corresponding flow loss are investigated firstly. Next, the performances of plasma actuations in suppressing the high-speed compressor cascade corner separation are studied. At last, the mechanisms behind the control effects of the suction surface and the endwall plasma actuations are discussed. Both the suction surface and the endwall plasma actuations can improve the high-speed compressor cascade static pressure rise coefficient, while reducing the corresponding total pressure loss and blockage coefficients. The suction surface plasma actuation can suppress not only the high-speed compressor cascade corner separation vortex but also the airfoil separation, so, compared to the endwall plasma actuation, the suction surface plasma actuation is more efficient in reducing the total pressure loss of the high-speed compressor cascade. However, through suppressing the development of the passage vortex, the endwall plasma actuation is more efficient in reducing the flow blockage and improving the static pressure rise of the high-speed compressor cascade.

Keywords: plasma actuation; active flow control; compressor; corner separation

1. Introduction

Corner separations always occur at the conjunctions between the compressor blade suction surface and the endwall. Modern gas-turbine engines are being designed with highly loaded compressors, and the associated strong adverse pressure gradient will cause the detrimental effects of corner separations to be unacceptable. In practice, it is these separations that greatly limit the compressor blade loading and efficiency by their impact on loss, blockage, and deviation [1–3].

Throughout the years, both the traditional passive and active flow control methodologies have been used to control the compressor corner separations. Passive flow control methodologies such as boundary layer fences [4,5], non-axisymmetric endwall contouring [6,7], and vortex generators [8–10] etc. can effectively reduce the detrimental effects of corner separations on the design conditions. However, at off-design conditions, extra flow mixing and separations induced by the passive methodologies may increase the flow blockage and loss. On the contrary, active flow control methodologies can be used to control the corner separations at the desired work conditions while being kept turned off at other work conditions to avoid bringing extra blockage and loss to the compressor flow field [11–14].

Plasma actuation is a typical active flow control methodology and has been proven to be capable of controlling both the compressor stall and corner separations effectively. Li et al. [15] experimentally studied the control effects of plasma actuation on the corner separations in a low-speed compressor cascade. Their results show that both steady and unsteady plasma actuation on the blade suction surface could control the corner separations effectively, and the unsteady plasma actuation achieved a better control effect. Based on their findings, they concluded that the unsteady plasma actuation could induce more vortex structures, and this was the reason that the unsteady plasma actuation could achieve a better control effect in suppressing the corner separations. Later, Wu and Zhao et al. [16–19] applied the plasma actuation to control the corner separations in a low-speed highly loaded compressor cascade. They used topological and vortex analysis theories to study the physical mechanisms of both the blade suction surface and the endwall plasma actuations in suppressing corner separation and found that the control effects of plasma actuations in suppressing corner separation are closely related to their ability to change the vortex structures within the corner separation. Giorgi et al. [20,21] also conducted a series of research on the control of compressor cascade flow separation with plasma actuation. They developed a micro plasma actuator and applied it to control the flow separation in a highly loaded subsonic compressor cascade and found that the plasma actuation could increase the pressure rise ability of the compressor cascade while decreasing the corresponding total pressure loss. Based on their findings, they concluded that increasing the actuation voltage can enhance the control effect of plasma actuation, but, from an energetic point of view, the plasma actuation with lower voltage is more efficient [21]. In 2016, Akcayoz et al. [22] published their studies on the plasma control of the compressor corner separation. They evaluated the effects of plasma actuations placed on the blade suction surface and the endwall respectively by suppressing the corner separation in a low-speed highly loaded compressor cascade with both numerical and experimental methods and found that the plasma actuators mounted upstream of the separation on both the suction surface and the endwall were most effective in suppressing the corner separation, while most of the improvement in total pressure loss stemmed from the suction surface actuator. Based on their research, it was concluded that, for the control of compressor corner separation, the required plasma actuator strength scaled approximately with the square of the Reynolds number.

In summary, researchers have spared a lot of efforts to uncover the flow control law and the mechanism behind the control of compressor corner separations with plasma actuations. These results laid solid foundations for the engineering applications of plasma actuations in controlling compressor corner separations. However, all the studies illustrated above are conducted in low-speed environments, and the performances of plasma actuations in controlling the high-speed compressor corner separations still remain unclear. One critical reason for the limitation of plasma actuator to suppress the corner separation in high-speed compressors should be the limited induced body forces. Recently, plasma actuation has been used by Saddoughi et al. [23] to control the stall of a transonic compressor by focusing on the control of the tip leakage flow. They adopted multiple dielectric barrier discharge (DBD) type plasma actuators, which can induce high magnitude velocity in quiescent air, in the experiments and successfully improved the stall margin of the transonic compressor. Hence, multiple DBD type plasma actuators may also be an effective tool for the control of endwall corner separations in high-speed compressors.

The main purpose of the present work is to uncover the flow control law and the mechanism of high-speed compressor cascade corner separation control with plasma actuations that consist of multiple DBD type plasma actuators. Both the suction surface and the endwall plasma actuations are used to control the corner separations in a high-speed compressor cascade. The main flow structures within the high-speed compressor cascade corner separation and the development of the corresponding flow loss are investigated firstly. Next, the performances of the plasma actuations in suppressing the high-speed compressor cascade corner separation are studied. According to the impact of plasma actuations on the flow structures within the high-speed compressor cascade corner separations, the mechanism behind the control effects of both the suction surface and the endwall plasma actuations are discussed in detail too.

2. Numerical Methods and Plasma Actuation Layouts

The typical high-speed compressor cascade, NACA65-K48, is studied. This high-speed compressor cascade model is designed by the research group DLR (German Aerospace Center) and has been used broadly to study the flow control of high-speed compressor cascade corner separations (see, for example, [4,5,8–10]). Its main geometrical and aerodynamic parameters are shown in Table 1.

Table 1. Main parameters of NACA65-K48 high-speed compressor cascade.

Main Parameters	Value
Chord (c)/mm	60
Span (h)/mm	100
Turning angle (θ)/°	42
Inlet flow angle (β_1)/°	132
Outlet flow angle (β_2)/°	90
Stagger angle (β_3)/°	112.5
Inlet Mach number	0.7
Solidity	0.55

Previously, Zhang et al. [24] have investigated the suitable RANS (Reynolds-averaged Navier-Stokes) numerical method to simulate the NACA65-K48 high-speed compressor cascade flow accurately and reliably. Based on their findings, the following numerical method is used in this paper to simulate the high-speed compressor cascade flow, and the comparisons between the experimental and numerical results, which can be found in reference [24], are omitted here.

The high-speed compressor cascade flow is simulated with Ansys CFX, and the calculation grid is established with ICEM. Figure 1 shows the calculation grid model. The topological structure of the calculation grid model is an H-O-H type, and the grid model consists of 2.8 million nodes. Grids near solid surfaces are refined to ensure $y^+ < 2$. To better simulate the influence of plasma actuation on the flow field, grids near plasma actuators are clustered. The two-equation k-ω eddy viscosity model is used to solve the Reynolds Stress in the RANS equations.

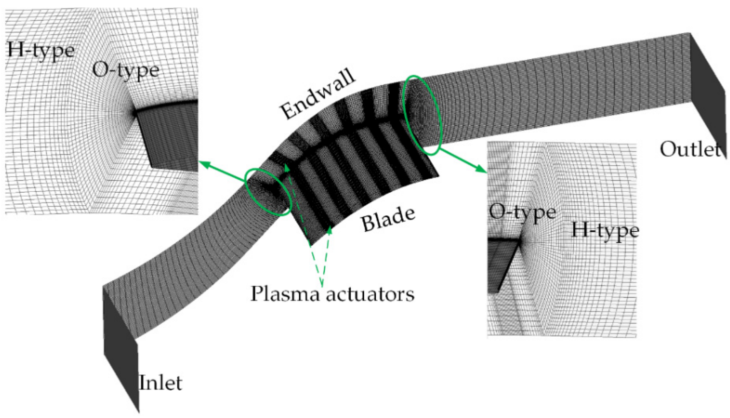

Figure 1. Calculation grid model.

According to the experimental study by Zhang et al. [24], for the incidences studied in this paper, the corner separation will not develop to the mid-span. Hence, the symmetrical boundary is used at mid-span to reduce the simulation cost. The inlet boundary is 1.5 chord lengths upstream of the blade's leading edge, and the outlet boundary is 2.5 chord lengths downstream of the blade's trailing edge. At the inlet, total pressure distributions along the spanwise direction together with a fixed total temperature from experiments (see for example in [24]) are imposed. At the outlet, the average static pressure boundary is applied to guarantee that the inlet Mach number is kept constant at 0.7 at different incidence angles. During the simulations, the fluid is treated as compressible and solid walls are treated as adiabatic and non-slipping.

Figure 2 shows the sketch of the DBD plasma actuator. Two electrodes are separated by the dielectric barrier, and when an AC voltage of several kilovolts is applied between the upper and lower electrodes, weakly ionized gases (plasma) are generated over the lower electrode in the air. As the plasma moves under the force of the electric field, it collides with the air. Through the momentum exchange within the collision, body force is imposed on the air. This paper uses the phonologic model developed by Suzen et al. [25] to simulate the body force induced by the plasma actuators. The accuracy of this model in simulating the body force of the plasma actuation has been validated by Suzen et al. [25] as well as Giorgi et al. [21], and, according to the discussion of Cork et al. [26], this model could qualitatively simulate the distribution of the body force of the plasma actuation.

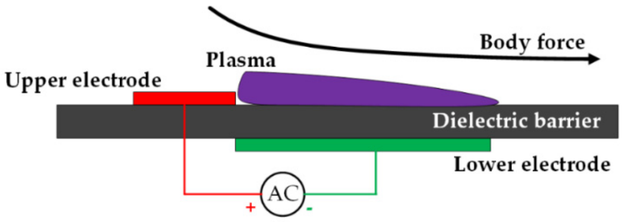

Figure 2. Sketch of the dielectric barrier discharge (DBD) plasma actuator.

Figure 3 shows the plasma actuation layouts studied in this paper. Both the suction surface and the endwall plasma actuation layouts consist of six plasma actuators. For each plasma actuator, the width of the upper and lower electrodes are 1 mm and 5 mm, respectively. On the blade suction surface, as indicated in Figure 3a, the first actuator SA1 is located 15% chord lengths downstream of the blade's leading edge, and the other five actuators, i.e. SA1–SA6, are placed at the downstream blade surface continuously, with an interval of 15% chord length in the chordwise direction. On the endwall surface, as depicted in Figure 3b, the six actuators, i.e. EA1–EA6, have the same layout as the blade suction surface actuators.

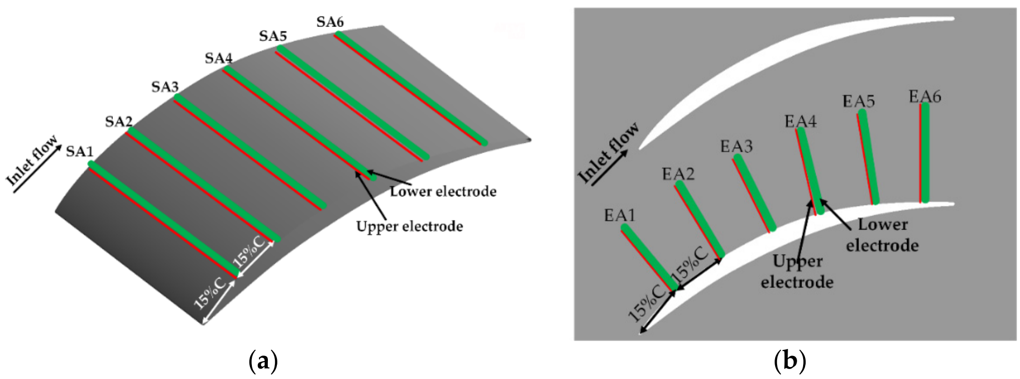

Figure 3. Plasma actuation layout. (**a**) Suction surface plasma actuation; (**b**) Endwall plasma actuation.

In this paper, a high voltage is imposed on the upper electrode, and the voltage of the lower electrode is set to zero. With these boundary conditions, the distribution of the electrostatic potential around the plasma actuator in the air is solved with Laplace's Equation:

$$\nabla(\varepsilon_r \nabla \Phi) = 0 \tag{1}$$

On the other hand, the spatial charge density is estimated on the basis of Poisson's equation:

$$\nabla(\varepsilon_{\mathrm{r}} \nabla \rho_c) = \rho_c \Big/ {\lambda_d}^2 \tag{2}$$

where ε_{r} is the relative permittivity of the air and λ_{d} is the Debye length.

The detailed introduction of the boundary condition to solve Laplace's and Poisson's equations as well as the values of the parameters can be found in reference [25]. With the results of Equations (1) and (2), the body force generated by the plasma actuator can be obtained:

$$F = \rho_c \cdot \vec{E} = \rho_c \cdot (-\nabla \Phi) \tag{3}$$

During the simulations, Equations (1) and (2) are solved firstly in quiescent air with user defined functions in Ansys CFX. Then the body force of the plasma actuator is calculated with Equation (3) and is applied as a boundary condition where plasma actuator of Figure 3 is located to control the high-speed compressor cascade flow separations.

Figure 4 shows the distribution of the induced velocity by the six plasma actuators in quiescent air with different body forces of plasma actuators. In this paper, the body forces of plasma actuators are changed through altering the high voltage imposed on the upper electrode. It can be found that, when the body force produced by a single plasma actuator reaches 837 mN/m, the maximum induced velocity of the six plasma actuators in quiescent air reaches around 30 m/s, and this is consistent with the multiple plasma actuators used by Saddoughi et al. [23]. This indicates that the overall plasma actuation strength can be realized with carefully designed multiple plasma actuators.

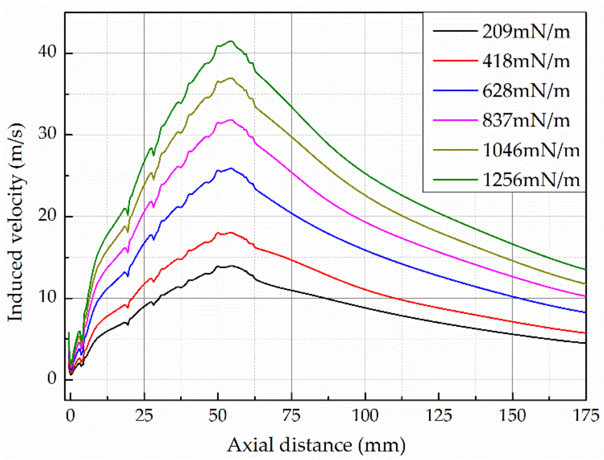

Figure 4. Distribution of induced velocity by six plasma actuators in quiescent air with different body forces of plasma actuators.

3. Results

To evaluate the control effects of plasma actuation in suppressing high-speed compressor cascade corner separations, the total pressure loss coefficient ω, static pressure rise coefficient, Cp, and the blockage coefficient, δ, are defined.

The total pressure loss coefficient ω is used to evaluate the flow loss and is defined as:

$$\omega = \frac{p_1 - p_2}{p_1 - p_{1s}} \tag{4}$$

where, p_1 and p_{1s} are the total pressure and static pressure of the incoming flow, respectively, and p_2 is the local total pressure.

The static pressure coefficient, *Cp,* is used to evaluate the pressure rise ability of the compressor cascade and is defined as:

$$Cp = \frac{p_{2s} - p_{1s}}{p_1 - p_{1s}} \tag{5}$$

where p_{2s} is the local static pressure.

The blockage coefficient, δ, is used to evaluate the flow blockage of the compressor cascade and is defined as:

$$\delta = 1 - \frac{v_x}{v_{mx}} \tag{6}$$

where v_{mx} is the axial velocity of the main flow stream.

To evaluate the overall flow loss in the cascade flow passage, the outlet plane mass averaged total pressure loss coefficient, ω_s, is defined as:

$$\omega_s = \frac{\iint \omega \rho v_x ds}{\iint \rho v_x ds} \tag{7}$$

where s is the area of the chosen plane and v_x is the axial velocity.

Similarly, the outlet plane area averaged static pressure rise, *Cps,* and the blockage coefficient, δ_s, are defined as:

$$Cp_s = \frac{\iint Cpds}{\iint ds} \tag{8}$$

$$\delta_s = \frac{\iint \delta ds}{\iint ds} \tag{9}$$

To evaluate the flow blockage at different blade heights, the pitch averaged flow blockage coefficient, δ_t, is defined as:

$$\delta_t = \sum_{i=1}^{n} (\delta_i \cdot \Delta t_i)/t \tag{10}$$

where t is the blade pitch.

In this paper, ω_s and *Cps* as well as δ_s and δ_t are all calculated at the plane 20% chord length downstream of the blade's trailing edge.

3.1. Flow Structures within the High-Speed Compressor Cascade Corner Separations and Development of the Corresponding Flow Loss

In this part, ten planes, p0–p9, which are vertical to the blade suction surface, are used to analyze the flow structures and the total pressure loss within the high-speed compressor cascade passage.

With the distributions of streamwise vorticity on planes p1–p9, Figure 5 shows the main flow structures within the high-speed compressor cascade corner separation and the development of the corresponding flow loss at the incidence angle of 0°. It can be found that the high-speed compressor cascade corner separation mainly consists of the passage vortex (PV), wall vortex (WV), free vortex (FV), corner vortex (CV), and trailing edge shedding vortex (TSV), and the development of the high-speed compressor cascade flow loss is closely related to the corner separation.

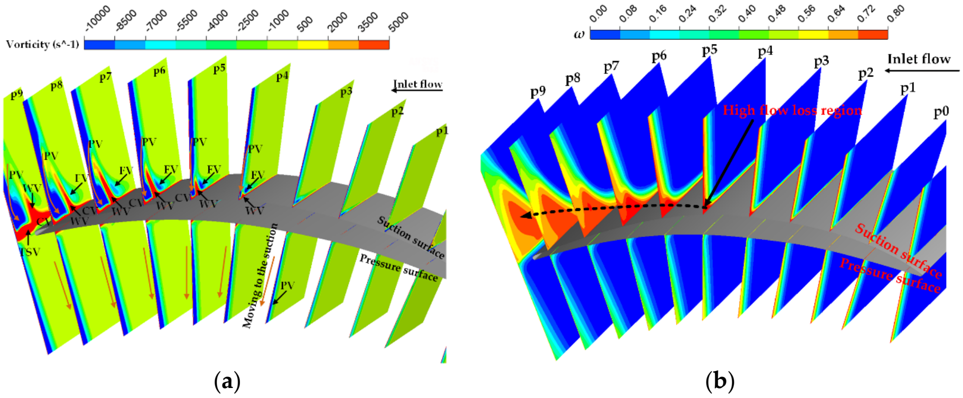

Figure 5. Flow structures within the high-speed compressor cascade corner separation and the development of the corresponding flow loss at an incidence angle of 0°. (**a**) Flow structures; (**b**) The development of flow loss.

As the endwall boundary layer moves to the suction surface, the PV arrives at the suction surface/endwall corner at plane p4. Then, the PV further extends to the midspan along the spanwise direction and increases in size, while moving downstream. In this procedure, the suction surface boundary layer is extruded by the PV, and the WV is formed resultantly. While moving downstream, the WV directly interacts with the main flow and determines the boundary of the high-speed compressor cascade corner separation. Meanwhile, it is pushed further and further away from the endwall by the PV and increases in size too. Under the influence of the WV, the FV is aroused from the main flow boundary layer, but it dissipates very quickly, while moving downstream. At plane p9, the FV is almost unobservable, while the PV and WV are still dominant flow structures within the high-speed compressor cascade corner separation. The CV exists around the suction surface/endwall corner, but its development is constrained by the PV, thus imposing limited influences on the high-speed compressor cascade flow. At the outlet of the high-speed compressor cascade passage, the flow from the pressure side encounters the corner separation and the TSV is aroused.

In summary, when the PV arrives at the suction surface/endwall corner, the high-speed compressor cascade corner separation occurs, and the flow structures of the high-speed compressor cascade corner separation are mainly determined by the development of the PV. Thus suppression of the PV seems key for the control of the high-speed compressor cascade corner separation. On the other hand, the boundary of the high-speed compressor cascade corner separation is mainly determined by the development of the WV, which indicates that the WV plays a crucial role in the interaction between the main flow and the corner separation. Thus suppression of the WV seems another key feature for the control of the high-speed compressor cascade corner separation.

According to Figure 5, a high flow loss region can be observed within the high-speed compressor cascade suction surface/endwall corner when the corner separation occurs. While moving downstream, the high flow floss region increases in size and strength with the development of the high-speed compressor cascade corner separation.

With the distributions of streamwise vorticity on planes p1–p9, Figure 6 shows the main flow structures within the high-speed compressor cascade corner separation and the development of the corresponding flow loss at the incidence angle of $-4°$. With Figures 5 and 6, it can be found, compared to the case with the incidence angle of 0°, that the location at which the corner separation occurs is located further away from the blade's leading edge and that the size of the high-speed compressor cascade corner separation is smaller with the incidence angle of $-4°$. Since the size of the high-speed compressor cascade corner separation is smaller with the incidence angle of $-4°$, the corresponding high flow loss region is more constrained to the corner region too. However, the developments of the PV, WV, FV, CV, and TSV, as well as the high flow loss region within the high-speed compressor cascade corner separation in Figure 6, still obey similar rules to those in

Figure 5. According to Figure 5, a high flow loss region can be observed near the blade pressure surface with the incidence angle of −4°, and this is caused by the pressure side flow separations at negative incidence angles.

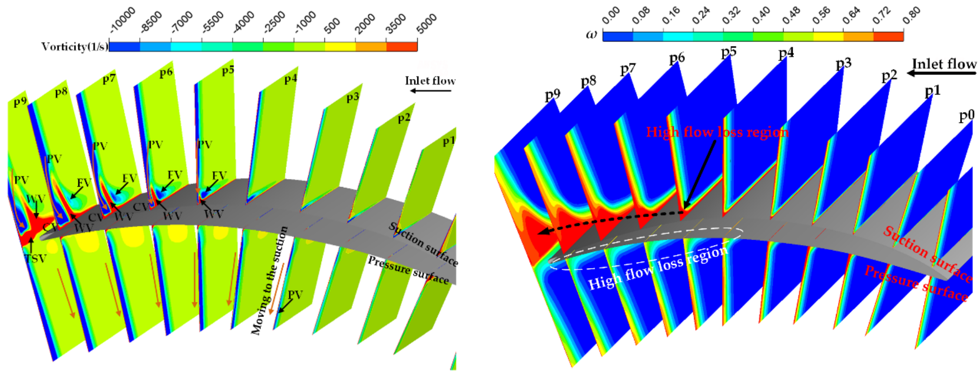

Figure 6. Flow structures within the high-speed compressor cascade corner separation and the development of the corresponding flow loss at an incidence angle of −4°. (**a**) Flow structures; (**b**) The development of flow loss.

With the distributions of streamwise vorticity on planes p1–p9, Figure 7 shows the main flow structures within the high-speed compressor cascade corner separation and the development of the corresponding flow loss at the incidence angle of 8°. With Figures 5 and 7, it can be found that, with the increase of the incidence angle, the occurrence of the high-speed compressor cascade corner separation becomes closer to the leading edge, and the size of the corner separation increases dramatically too. As a result, the high-speed compressor cascade flow loss is increased simultaneously. However, the developments of the PV, WV, FV, CV, and TSV, as well as the high flow loss region within the high-speed compressor cascade corner separation in Figure 7, still obey similar rules to those in Figures 5 and 6.

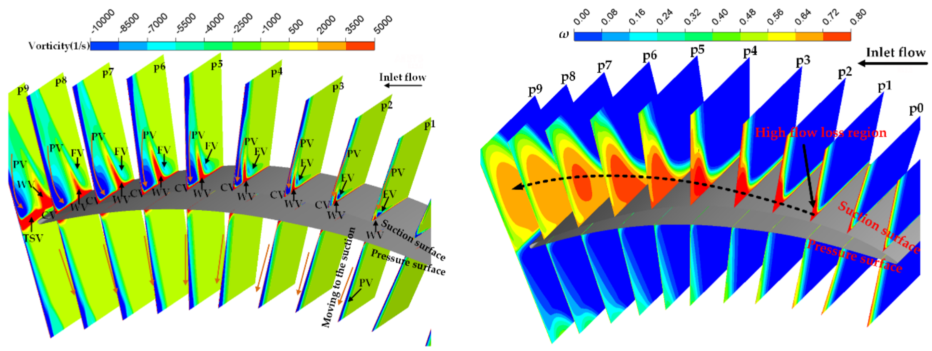

Figure 7. Flow structures within the high-speed compressor cascade corner separation and the development of the corresponding flow loss at an incidence angle of 8°. (**a**) Flow structures; (**b**) The development of flow loss.

3.2. Performances of Plasma Actuations in Suppressing the High-Speed Compressor Cascade Flow Separation

3.2.1. Influences of Plasma Actuations on the High-Speed Compressor Cascade Flow Loss at Different Streamwise Planes

Figure 8 shows the influences of plasma actuations on the high-speed compressor cascade flow loss at different streamwise planes. The $\Delta\omega$ is obtained through the subtraction of the total pressure loss coefficient of baseline condition from the plasma actuations, and the positive value in the figure indicates that the total pressure loss coefficient is reduced by the plasma actuations. The corresponding body force of each single plasma actuator in Figure 8 is confined to 837 mN/m.

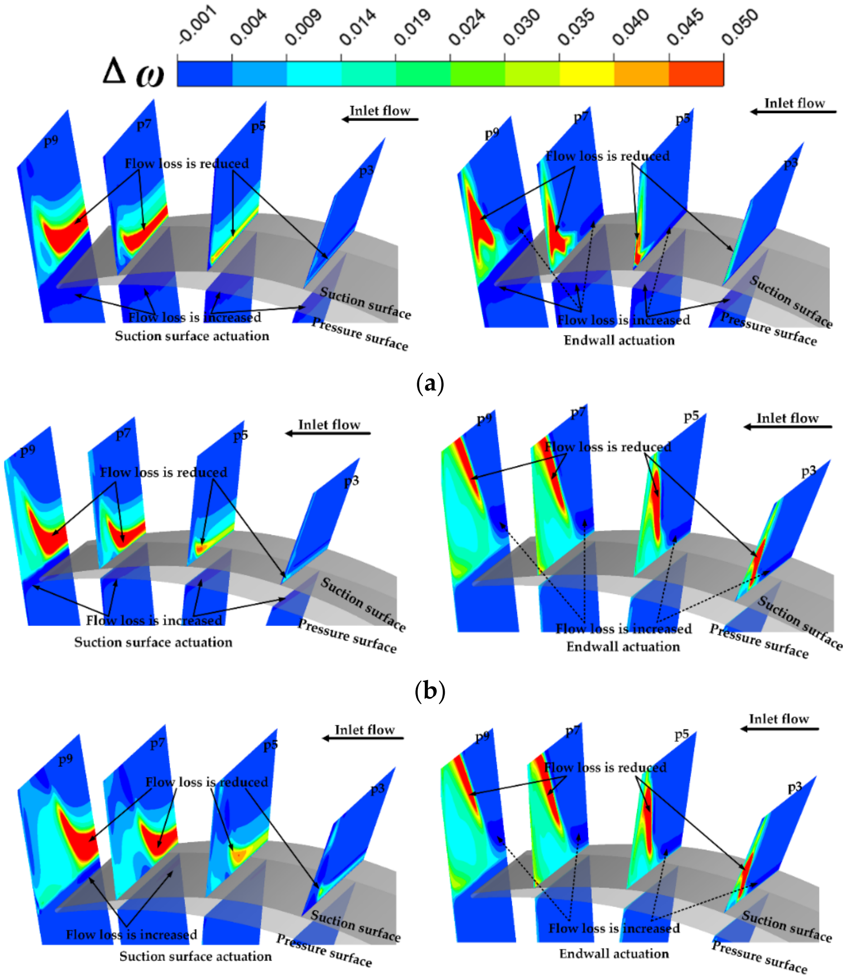

Figure 8. Influences of plasma actuations on the high-speed compressor cascade flow loss at different streamwise planes. (**a**) With an incidence angle of −4°; (**b**) With an incidence angle of 0°; (**c**) With an incidence angle of 8°.

Based on Figures 5–8, it can be found that the influences of the suction surface and the endwall plasma actuations on the high-speed compressor cascade flow loss are closely related to the developments of the corner separations. When the high-speed compressor cascade corner separation occurs, the corresponding flow loss is obviously reduced by both the suction surface and the endwall plasma actuations. However, the locations and shapes of the regions where the suction surface and endwall plasma actuations reduce the flow loss are quite different. This phenomenon will be discussed later in this paper.

According to Figure 8, the area of the regions where the high-speed compressor cascade flow loss is reduced by both the suction surface and the endwall plasma actuations keeps almost constant with the increase of incidence angles, and this is because the scope of the influences of plasma actuations is limited to the regions near solid walls. Since the strength and size of the high-speed compressor cascade corner separation increases dramatically with the increase of incidence angles, it can be concluded that the plasma actuation will impose a relatively smaller influence on the high-speed compressor cascade corner separations of large positive incidence angles than on that of smaller and negative incidence angles.

As the high-speed compressor cascade corner separation is suppressed by the plasma actuations, the overall blockage of the cascade flow is reduced. As a result, the flow loss outside the high-speed compressor cascade corner separation region will be increased by the plasma actuations. Especially at negative incidence angles, as shown in Figure 8a, the original pressure side separations are obviously enhanced by both the suction surface and endwall plasma actuations. On the other hand, the endwall plasma actuation increases the flow loss near mid-span regions too, and this indicates that the endwall plasma actuation is incapable of suppressing the airfoil separations, which will be discussed later in this paper.

3.2.2. Influences of Plasma Actuations on the High-Speed Compressor Cascade Outlet Flow Loss, Static Pressure Rise and Blockage

Figure 9 shows the influences of plasma actuations on the high-speed compressor cascade total pressure loss, static pressure rise, and blockage coefficients at different incidence angles. The positive value of the relative variation rate of *Cps* represents the relative increase of the plane area averaged static pressure rise coefficient, while the positive values of the relative variation rate of ω_s and δs represent the relative decrease of the plane mass averaged total pressure loss coefficient and the plane area averaged blockage coefficient, respectively. The corresponding body force of each single plasma actuator shown in Figure 9 is confined to 837 mN/m.

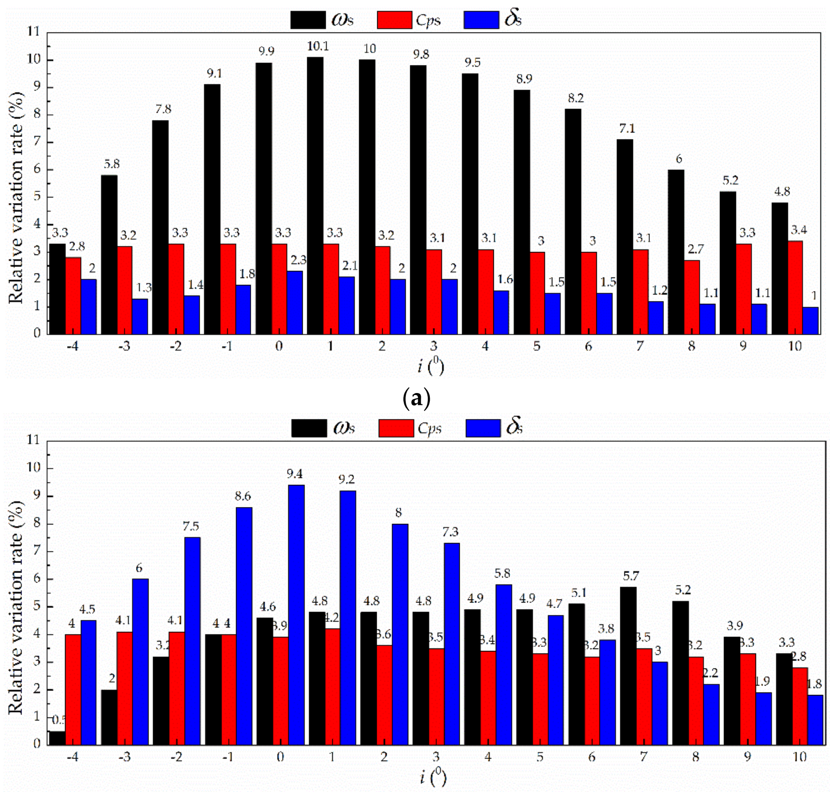

(a)

(b)

Figure 9. Influences of plasma actuations on the high-speed compressor cascade total pressure loss, static pressure rise, and blockage coefficients at different incidences. (**a**) Suction surface plasma actuation; (**b**) Endwall plasma actuation.

According to Figure 9a, the influences of the suction surface plasma actuation on the high-speed compressor cascade static pressure rise coefficient vary slightly with the change of incidence angles.

It can be found the static pressure rise coefficient of the high-speed compressor cascade achieves a relative increase of 3% with the suction surface plasma actuation. However, the incidence angle imposes a remarkable influence on the control effects of the suction surface plasma actuation in reducing the high-speed compressor cascade total pressure loss and blockage coefficients. At an incidence angle of 1°, the total pressure loss coefficient of the high-speed compressor cascade achieves a maximum relative reduction of 10.1% with the suction surface plasma actuation. With the increase of incidence angles, strength of the high-speed compressor cascade corner separation is enhanced, and the ability of the suction surface plasma actuation to reduce the corresponding total pressure loss thus decreases. The scope of the influence of plasma actuation is limited to the regions near solid walls, and this leads to the inefficiency of the suction surface plasma actuation in reducing the total pressure loss of large-scale high-speed compressor cascade corner separations at large positive incidence angles. With the decrease of incidence angles, the strength of the high-speed compressor cascade corner separation is weakened, and the pressure side separation contributes more and more to the overall total pressure loss of the high-speed compressor cascade flow. As a result, the ability of the suction surface plasma actuation to reduce the total pressure loss at negative incidence angles decreases too. At an incidence angle of 0°, the blockage coefficient of the high-speed compressor cascade achieves a maximum relative reduction of 2.3% with the suction surface plasma actuation. With the change of incidence angles, the variance of the influences of the suction surface plasma actuation on the high-speed compressor cascade blockage coefficient obeys a similar rule to its influences on the high-speed compressor cascade total pressure loss coefficient discussed above.

According to Figure 9b, compared to the work conditions of large positive incidence angles, the endwall plasma actuation imposes stronger influences on the high-speed compressor cascade static pressure rise coefficients at negative and small positive incidence angles. At an incidence angle of 1°, the static pressure rise coefficient of the high-speed compressor cascade achieves a maximum relative increase of 4.2% with the endwall plasma actuation. At an incidence angle of 7°, the total pressure loss coefficient achieves a maximum relative reduction of 5.7% with the endwall plasma actuation. Then, similar to the case of the suction surface plasma actuation, with the increase and decrease of incidence angles, the reduction of the high-speed compressor cascade total pressure loss coefficient and the endwall plasma actuation both decrease. However, the endwall plasma actuation imposes stronger influences on the high-speed compressor cascade total pressure loss coefficient at large positive incidence angles than at small positive and negative incidence angles. In practice, at large positive incidence angles, the corner separation contributes the most to the total pressure loss of the high-speed compressor cascade, while, at small positive and negative incidence angles, the airfoil loss of pressure and suction side separations will play a more important role in producing the total pressure loss of the high-speed compressor cascade. Compared to the suction surface plasma actuation, the endwall plasma actuation is much more efficient in reducing the total pressure loss of corner separations and less efficient in reducing the total pressure loss of airfoil separations. At an incidence angle of 0°, the blockage coefficient of the high-speed compressor cascade achieves a maximum relative reduction of 9.4%. Then, similar to the case of the suction surface plasma actuation, with the increase and decrease of incidence angles, the reduction of the high-speed compressor cascade blockage coefficient and the endwall plasma actuation both decrease.

From Figure 9a,b, it can be found that the suction surface plasma actuation is more efficient in reducing the total pressure loss coefficient of the high-speed compressor cascade, while the endwall plasma actuation is more efficient in reducing the blockage coefficient and increasing the static pressure rise coefficient of the high-speed compressor cascade. These phenomena are associated with the mechanisms behind the control effects of plasma actuation in suppressing the high-speed compressor cascade flow separation, which will be discussed later.

3.3. Influences of Body Force on the Control Effects of Plasma Actuation in Suppressing High-Speed Compressor Cascade Corner Separation

Figure 10 shows the influences of plasma actuations on the high-speed compressor cascade total pressure loss and blockage coefficients, with plasma actuators inducing different body forces. The inlet flow incidence angle of the high-speed compressor cascade is confined to 0° in Figure 10.

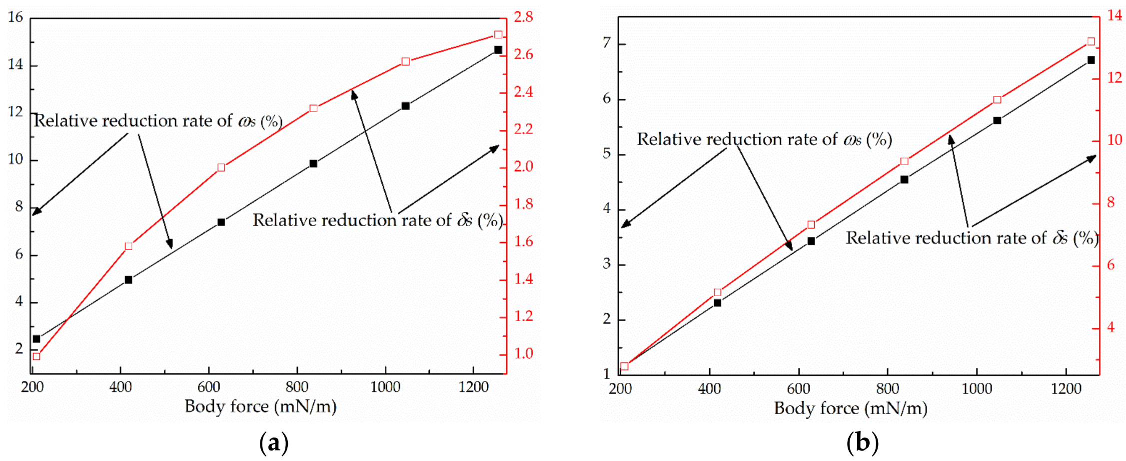

Figure 10. Influences of plasma actuations on the high-speed compressor cascade total pressure loss and blockage coefficients, with plasma actuators inducing different body forces. (**a**) Suction surface plasma actuation; (**b**) Endwall plasma actuation.

According to Figure 10a, with the increase of the body forces of plasma actuators, the relative reduction rate of the high-speed compressor cascade total pressure loss coefficient with the suction surface plasma actuation increases linearly, while the corresponding relative reduction rate of the high-speed compressor cascade blockage coefficient increases more and more slowly. According to Figure 10b, with the increase of the body forces of plasma actuators, the relative reduction rate of the high-speed compressor cascade total pressure loss and blockage coefficients with the endwall plasma actuation both increase linearly.

Based on Figure 10a, it can be found that the control effects of plasma actuation in suppressing high-speed compressor cascade corner separation are not always linearly correlated with the body forces of plasma actuators. Two factors are responsible for this phenomenon. First, the scope of the influence of the suction surface plasma actuation is limited to the region near solid walls and cannot be directly enlarged with the increase of the body forces of plasma actuators. On the other hand, the corner separation is highly three-dimensional and always extends far away from the solid walls. As a result, when the body forces of the plasma actuators are increased, the ability of the suction surface plasma actuation to reduce the high-speed compressor cascade corner separation blockage is limited.

3.4. Mechanisms behind the Control Effects of Plasma Actuations in Suppressing High-Speed Compressor Cascade Corner Separation

Figure 11 shows the influences of plasma actuations on the total pressure at plane p6 and on the corresponding main flow structures. In Figure 11b,c, the variance of total pressure is obtained through the subtraction of the total pressure of baseline condition and from the plasma actuations, and the positive value in the figure indicates that plasma actuation improves the flow total pressure.

According to Figure 11b,c, both the suction surface and the endwall plasma actuations can improve the total pressure of the high-speed compressor cascade flow, but the regions where the flow total pressure is improved are obviously different for these two plasma actuation layouts. From Figure 11a,b, it can be found that the suction surface plasma actuation improves the total pressure of the high-speed compressor cascade flow mainly through suppressing the airfoil separation and the WV, as well as its interaction with the FV. However, from Figure 11a,c, it can be found that the endwall plasma actuation improves the total pressure of the high-speed compressor cascade flow mainly through suppressing the PV, as well as its interaction with the WV. Since the mechanisms behind the control effects of the suction surface and the endwall plasma actuation in suppressing the high-speed compressor cascade corner separation are different, their behaviors in Figures 9 and 10 are resultantly different too.

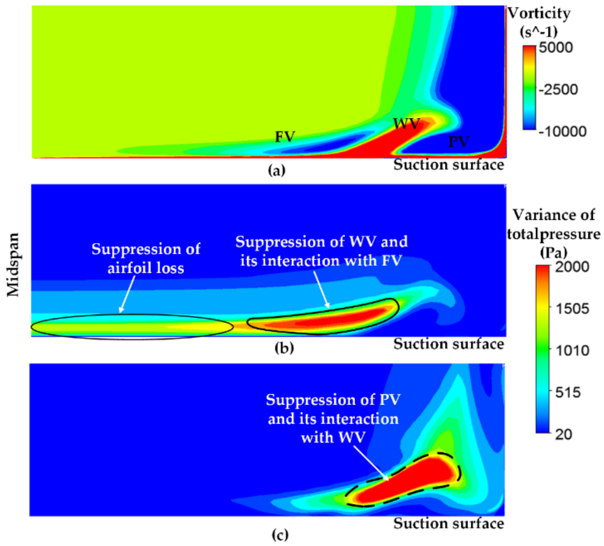

Figure 11. Influences of plasma actuations on the total pressure at plane p6 and the corresponding main flow structures. (**a**) Main flow structures at plane p6 of baseline condition; (**b**) Variance of total pressure with the suction surface plasma actuation; (**c**) Variance of total pressure with the endwall plasma actuation.

Figure 12 shows the influences of plasma actuations on the pitch-averaged blockage coefficients of the high-speed compressor cascade. According to Figure 12a, strong flow blockage can be observed within the core region of the high-speed compressor cascade corner separation, and the flow blockage at the boundary of the corner separation is slightly reduced by the suction surface plasma actuation, which is associated with the suppression of the WV. On the contrary, as shown in Figure 12b, flow blockage within the core region of the high-speed compressor cascade corner separation is obviously reduced by the endwall plasma actuation, which is associated with the suppression of the PV.

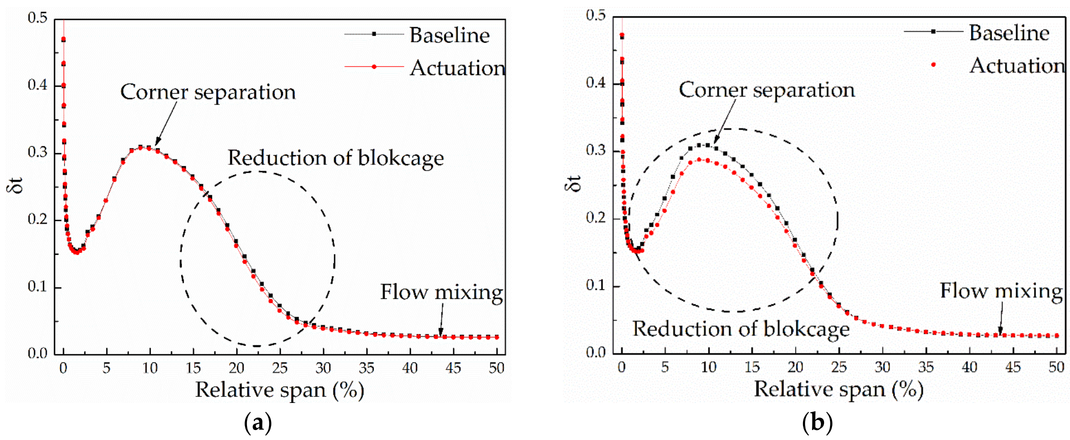

Figure 12. Influences of plasma actuations on the pitch-averaged blockage coefficients of the high-speed compressor cascade. (**a**) Suction surface plasma actuation; (**b**) Endwall plasma actuation.

4. Discussion and Conclusions

Both the suction surface and the endwall plasma actuations can improve the high-speed compressor cascade static pressure rise coefficient, while reducing the corresponding total pressure loss and blockage coefficients. The ability of the plasma actuations to improve the high-speed compressor cascade static pressure rise coefficient is slightly influenced by the incidence angles. However, the abilities of the plasma actuations to reduce the high-speed compressor cascade total pressure loss and blockage coefficients are closely related to the incidence angles. At negative incidence angles, the pressure side separation plays a very important role in the generation of the high-speed compressor cascade total pressure loss and blockage coefficients. As a result, the suction surface and the endwall plasma actuations are quite inefficient in reducing the high-speed compressor cascade total pressure loss as well as blockage coefficients. In future studies, the pressure side plasma actuation may be used to control the high-speed compressor cascade flow separation at negative incidence angles. At large positive incidence angles, both the suction surface and the endwall plasma actuations are very inefficient in suppressing the high-speed compressor cascade corner separations at large scales too. The fact that the scope of the influence of plasma actuations is limited to the regions near solid surfaces is responsible for this phenomenon. For the same reason, with the increase of the body forces of plasma actuators, the relative reduction rate of the high-speed compressor cascade blockage coefficient increases more and more slowly with the suction surface plasma actuation. Thus, in future studies, a brand new three-dimensional plasma actuator, which can influence flow fields far away from solid walls, may be used to control the high-speed compressor cascade corner separations at large scales.

The suction surface plasma actuation can suppress not only the high-speed compressor cascade corner separation vortex (WV) but also the airfoil separation, so it is more efficient in reducing the total pressure loss of the high-speed compressor cascade. This finding is in accordance with the results of Akcayoz et al. [22], which point out that, compared with the endwall plasma actuation, the plasma actuation on the blade suction surface contributes the most to the improvement in the total pressure loss of the compressor cascade. However, this paper finds that, through suppressing the development of the PV, the endwall plasma actuation is more efficient in reducing the flow blockage and improving the static pressure rise of the high-speed compressor cascade. As a matter of fact, the PV is the main flow structure that determines the characteristics of the high-speed compressor cascade corner separations. Since the formation and development of the PV are determined by the movement of endwall boundary layer, the suction surface plasma actuation is incapable of influencing the PV effectively. Thus it can be concluded that the endwall plasma actuation is more efficient in suppressing the high-speed compressor cascade corner separation than the suction surface plasma actuation. In future studies, based on the mechanisms by which they control the high-speed compressor cascade flow, both the suction surface and the endwall plasma actuation layouts should be optimized to obtain better control effects, while minimizing the power consumption.

Acknowledgments: This paper was supported by the National Natural Science Foundation of China (Nos. 51336011, 51376014, 51476004). Thanks go to Robert Meyer of DLR for advising on the NACA65-K48 airfoil data.

Author Contributions: Haideng Zhang performed the simulations and wrote the paper. Xianjun Yu and Bojie Liu contributed to the analysis of the simulation results. Yun Wu and Yinghong Li contributed to the design of the plasma actuation layouts.

Conflicts of Interest: The authors declare no conflict of interest.

References

1. Gbadebo, S.A.; Cumpsty, N.A.; Hynes, T.P. Three-dimensional separations in axial compressors. *J. Turbomach.* **2005**, *127*, 331–339. [CrossRef]
2. Goodhand, M.N.; Miller, R.J. The impact of real geometries on three-dimensional separations in compressors. *J. Turbomach.* **2010**, *134*, 021007. [CrossRef]

3. Gao, F.; Ma, W.; Zambonini, G.; Boudet, J.; Ottavy, X.; Lu, L.; Shao, L. Large-eddy simulation of 3-D corner separation in a linear compressor cascade. *Phys. Fluids* **2015**, *27*, 354–363. [CrossRef]
4. Hergt, A.; Meyer, R.; Karl, E.; Nicke, E. A new approach for compressor endwall contouring. In Proceedings of the ASME 2011 Turbo Expo: Turbine Technical Conference and Exposition, Vancouver, BC, Canada, 6–10 June 2011; pp. 45177–45186.
5. Liesner, K.; Meyer, R. Combination of active and passive flow control in a high speed compressor casacade. In Proceedings of the ASME Turbo Expo 2014: Turbine Technical Conference and Exposition, Düsseldorf, Germany, 16–20 June 2014.
6. Dorfner, C.; Hergt, A.; Nicke, E.; Moenig, R. Advanced non-axisymmetric endwall contouring for axial compressors by generating an aerodynamic separator-part I: Principal cascade design and compressor application. In Proceedings of the ASME Turbo Expo 2009: Power for Land, Sea, and Air, Orlando, FL, USA, 8–12 June 2009; pp. 59113–59120.
7. Hergt, A.; Dorfner, C.; Steinert, W.; Nicke, E.; Schreiber, H.-A. Advanced non-axisymmetric endwall contouring for axial compressors by generating an aerodynamic separator-part II: Experimental and numerical cascade investigation. In Proceedings of the ASME Turbo Expo 2009: Power for Land, Sea, and Air, Orlando, FL, USA, 8–12 June 2009; pp. 59121–59131.
8. Hergt, A.; Meyer, R.; Engel, K. Experimental investigation of flow control in compressor cascades. In Proceedings of the ASME Turbo Expo 2006: Power for Land, Sea, and Air, Barcelona, Spain, 8–11 May 2006; pp. 90231–90240.
9. Hergt, A.; Meyer, R.; Müller, M.W.; Engel, K. Loss reduction in compressor cascades by means of passive flow control. In Proceedings of the ASME Turbo Expo 2008: Power for Land, Sea, and Air, Berlin, Germany, 30 June 2008; pp. 50269–50280.
10. Hergt, A.; Meyer, R.; Engel, K. Effects of vortex generator application on the performance of a compressor cascade. *J. Turbomach.* **2012**, *135*, 021026. [CrossRef]
11. Gbadebo, S.A.; Cumpsty, N.A.; Hynes, T.P. Control of three-dimensional separations in axial compressors by tailored boundary layer suction. *J. Turbomach.* **2007**, *130*, 011004. [CrossRef]
12. Hecklau, M.; Wiederhold, O.; Zander, V.; King, R.; Nitsche, W.; Swoboda, M.; Huppertz, A. Active separation control with pulsed jets in a critically loaded compressor cascade. *AIAA J.* **2011**, *49*, 1729–1739. [CrossRef]
13. Evans, S.; Hodson, H. Separation-control mechanisms of steady and pulsed vortex-generator jets. *J. Propul. Power* **2012**, *28*, 1201–1213. [CrossRef]
14. Gmelin, C.; Zander, V.; Huppertz, A.; Swoboda, M.; Hecklau, M.; Thiele, F.; Nitsche, W. Active flow control concepts on a highly loaded subsonic compressor cascade: Résumé of experimental and numerical results. *J. Turbomach.* **2012**, *134*, 061021. [CrossRef]
15. Li, Y.H.; Wu, Y.; Zhou, M.; Su, C.B.; Zhang, X.W.; Zhu, J.Q. Control of the corner separation in a compressor cascade by steady and unsteady plasma aerodynamic actuation. *Exp. Fluids* **2010**, *48*, 1015–1023. [CrossRef]
16. Wu, Y.; Zhao, X.H.; Li, Y.H.; Li, J. Corner separation control in a highly loaded compressor cascade using plasma aerodynamic actuation. In Proceedings of the ASME Turbo Expo 2012: Turbine Technical Conference and Exposition, Copenhagen, Denmark, 11–15 June 2012; pp. 69323–69332.
17. Zhao, X.; Li, Y.; Wu, Y.; Zhu, T.; Li, Y. Numerical investigation of flow separation control on a highly loaded compressor cascade by plasma aerodynamic actuation. *Chin. J. Aeronaut.* **2012**, *25*, 349–360. [CrossRef]
18. Zhao, X.H.; Wu, Y.; Li, Y.H.; Wang, X.D.; Zhao, Q. Topological analysis of plasma flow control on corner separation in a highly loaded compressor cascade. *Acta Mech. Sin.* **2012**, *28*, 1277–1286. [CrossRef]
19. Zhao, X.; Li, Y.; Wu, Y.; Li, J. Investigation of endwall flow behavior with plasma flow control on a highly loaded compressor cascade. *J. Therm. Sci.* **2012**, *21*, 295–301. [CrossRef]
20. Giorgi, M.G.D.; Traficante, S.; Luca, C.D.; Bello, D.; Ficarella, A. Active flow control techniques on a stator compressor cascade: a comparison between synthetic jet and plasma actuators. In Proceedings of the ASME Turbo Expo 2012: Turbine Technical Conference and Exposition, Copenhagen, Denmark, 11–15 June 2012; pp. 69439–69450.
21. Giorgi, M.G.D.; Pescini, E.; Marra, F.; Ficarella, A. Experimental and numerical analysis of a micro plasma actuator for active flow control in turbomachinery. In Proceedings of the ASME Turbo Expo 2014: Turbine Technical Conference and Exposition, Düsseldorf, Germany, 16–20 June 2014.
22. Akcayoz, E.; Vo, H.D.; Mahallati, A. Controlling corner stall separation with plasma actuators in a compressor cascade. *J. Turbomach.* **2016**, *138*, 081008. [CrossRef]

23. Saddoughi, S.; Bennett, G.; Boespflug, M.; Puterbaugh, S.L.; Wadia, A.R. Experimental investigation of tip clearance flow in a transonic compressor with and without plasma actuators. *J. Turbomach.* **2014**, *137*, 041008. [CrossRef]
24. Zhang, H.; Wu, Y.; Li, Y.; Lu, H. Experimental investigation on a high subsonic compressor cascade flow. Chin. *J. Aeronaut.* **2015**, *28*, 1034–1043. [CrossRef]
25. Suzen, Y.; Huang, G.; Jacob, J.; Ashpis, D. Numerical simulations of plasma based flow control applications. In Proceedings of the 35th AIAA Fluid Dynamics Conference and Exhibit, Toronto, ON, Canada, 6–9 June 2005; pp. 2005–4633.
26. Corke, T.C.; Enloe, C.L.; Wilkinson, S.P. Dielectric barrier discharge plasma actuators for flow control. *Annu. Rev. Fluid Mech.* **2010**, *42*, 505–529. [CrossRef]